A MINIMUM COMPLEXITY MODEL FOR THE AEROELASTIC ANALYSIS OF DISTRIBUTED PROPULSION AIRCRAFT

Aykut Tamer[†], Ali Tatar[‡,*]
[†]University of Bath, UK
[‡]Leonardo Helicopters, UK

[*] ali.tatar@leonardo.com

Abstract

An important number of recent urban mobility aircraft have multiple propellers to generate the required levels of power for electric propulsion. The novel urban mobility designs are expected to exhibit more complex aeroelastic behaviour with their multiple propellers distributed over the aircraft structure because of the aeroelastic instabilities such as whirl flutter and wing flutter. While it is possible to use sophisticated numerical simulations to address the aeroelastic instabilities in distributed propulsion aircraft, they are difficult to use in early design stages due to a lack of data and their computational cost when experimenting over a wide range of parameters is required. On the other hand, aeroelastic problems cannot be oversimplified due to their multidisciplinary nature. Therefore, a minimum complexity model is required for the aeroelastic analysis of distributed propulsion aircraft by combining structural and aerodynamic models of the wing and multiple propellers, which is less complex than sophisticated tools yet good enough to capture the instabilities. For this purpose, the authors developed a minimum complexity model for the aeroelastic analysis of such aircraft. In the proposed aeroelastic model, the wing structure is built using a finite volume beam formulation. The unsteady aerodynamics of the wing is based on Wagner‘s function and formulated for wing sections. Finally, the classical Reed‘s model is used for the aeroelastic modelling of the propellers. The model is verified against results in the literature and its benefits are further demonstrated through sample analysis.

Introduction

In recent years, there has been a significant increase in the development of novel electric distributed propulsion aircraft configurations due to the aerodynamic efficiency, reduced noise and emission targets of aircraft manufacturers [1]. On the other hand, multiple propellers and flexible wing structure interaction in the distributed propulsion aircraft results in a coupled aeroelastic problem with various aeroelastic instabilities such as whirl flutter and wing flutter [2]. Therefore, aeroelastic modelling of distributed propulsion aircraft for an accurate dynamic response prediction has recently become an important research topic. To understand the whirl flutter stability of distributed propulsion aircraft, a significant number of studies have been conducted on the NASA Aircraft X-57 with a specific focus on the whirl flutter [3]. Furthermore, the aeroelastic coupling between whirl flutter and wing flutter modes has been investigated in the recent papers [4, 5].

Whirl flutter is a well-known dynamic instability problem in rotorcraft aeromechanics. Fundamentally, aerodynamic and gyroscopic moments acting on the propeller-rotor lead to this instability problem when the stiffness or damping between the propeller-rotor and nacelle is not adequate [6, 7]. The resulting instability can act as a limiting factor in fixed-wing and tilt-rotor aircraft performance. In the current industry practice, rotors are expected to operate away from whirl flutter conditions [8]. So far, a large amount of research has been conducted to understand whirl flutter stability and its boundaries [9]. The so-called whirl flutter is more complicated than the classical fixed-wing flutter due to the inclusion of gyroscopic moments. In whirl flutter prediction, Reed‘s [10] and Johnson‘s models [11] are widely used to predict the whirl flutter stability of propellers. The so-called Reed‘s model has basically two degrees of freedom, including the pitching and yawing motions with the gyroscopic and aerodynamic moments in these directions. Moreover, Johnson‘s model includes rotor-blade, pylon and wing dynamics.

Novel aircraft have different architectures [1] and most of them possess multiple propellers (distributed propulsion) to benefit from electrical propulsion as seen in Fig. 1. It is important to address whirl-flutter in these architectures as it is required in similar conventional turboprop and tiltrotor aircraft, which require proper tools. While it is possible to benefit from advanced simulation techniques to predict stability boundaries [12, 13], simpler methods are also advantageous for quick estimations during early design stages to scan a large design space and perform sensitivity analysis. One such model is 2DOF Reed’s whirl-flutter model, which has been extensively used for the whirl-flutter stability analysis.

The main aim of this paper is to present an aeroelastic model of distributed propulsion aircraft with a minimum complexity level. This basic aeroelastic model is able to predict both whirl flutter and wing flutter without using the sophisticated finite element method and computational fluid dynamics tools, which significantly reduces computational costs for optimisation studies in the early design stages of urban air mobility vehicles. For this purpose, finite volume method-based beam formulation and unsteady aerodynamics theory based on Wagner's function are employed for structural and aerodynamics modelling of the wing, respectively. Multi propeller aeroelastic model is also developed, which is an extended version of Reed's model for an arbitrary number of propellers. The full aeroelastic model of distributed propulsion aircraft with the minimum complexity described in this paper can be easily created in popular programming languages such as Matlab, Python etc. It can be used as a design tool in the stability analysis of distributed propulsion air vehicles.

Figure 1: A distributed propulsion aircraft [14]

Method

This section explains the techniques to model the aeroelastic problem distributed propulsion system focusing on the least complex methods. The overall model is composed of blending propellers and wing, as explained next.

Wing Structure

The simplest way of modelling a wing is using beam formulation. While there are lumped parameter models, their formulation is not simpler than beam models, especially considering possible couplings between different motions of a wing such as bending and torsion. A physically sound way is the Finite Volume concept, which is based on the direct balance of forces and moments on a finite volume of solid rather than using the weak formulation of strain energy. The finite volume formulation of Ref. [15] is implemented to obtain the structural dynamics representation in its linear form [16].

The beam is discretised using three nodes, each node possessing three translational and three rotational degrees of freedom. For a beam element, the equilibrium of internal forces at two internal points and external forces at the three nodes are written and linearised. The internal loads are related to the internal strains using a 6×6 stiffness matrix. Then, the linearised strain terms are written as a function of node degrees of freedom using interpolation polynomials.

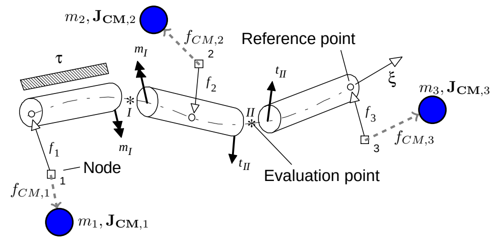

Figure 2: 3-node Beam element.

The 3-node beam element is shown in Fig. 2. The reference plane, at which elastic properties are defined is named as *material reference frame* and lies on a dimensionless coordinate ξ, has orientation $\mathbf{R}$ with respect to the blade reference frame, allowing ease in defining elastic properties such as defining the constitutive law about principal axis. The nodes, $(i = 1,2,3)$ are the locations where position $(\mathbf{p})$ and curvature (κ) about three orthogonal axes are represented and external loads are applied. The strains and internal loads are computed at the evaluation points, which are represented by Roman footers $(k = I, II)$, as shown in Fig. 2. The equation of beam can be stated as an equilibrium between the internal forces and moment (ϑ) and the distributed forces and moments (τ);

$$\vartheta' - \mathbf{T}^T\vartheta + \tau = 0 \tag{1}$$

where derivation is evaluated with respect to beam reference line ξ and $\mathbf{T}^T$ is the arm matrix of internal forces:

$$\mathbf{T} = \begin{bmatrix} 0 & \mathbf{p}'\times \\ 0 & 0 \end{bmatrix} \tag{2}$$

The internal loads $(\vartheta = [\vartheta_I^T \ \ \vartheta_{II}^T]^T)$ evaluated at the evaluation points and the external loads $(\mathbf{F} = [\mathbf{F}_1^T \ \ \mathbf{F}_2^T \ \ \mathbf{F}_3^T]^T)$ applied at node points are in equilibrium according to the formulation [15];

$$\mathbf{A}\vartheta = \mathbf{F} \tag{3}$$

where $\mathbf{A}$ is the integrated arms matrix (Eq. 1) which guarantees equilibrium between the external loads at the nodes and internal loads at the evaluation points.

$$\mathbf{A} = \begin{bmatrix} \mathbf{I} & \mathbf{0} & \mathbf{0} & \mathbf{0} \\ (\mathbf{p}_I - \mathbf{x}_1)\times & -\mathbf{I} & \mathbf{0} & \mathbf{0} \\ \mathbf{I} & \mathbf{0} & -\mathbf{I} & \mathbf{0} \\ -(\mathbf{p}_I - \mathbf{x}_2)\times & \mathbf{I} & (\mathbf{p}_{II} - \mathbf{x}_1)\times & -\mathbf{I} \\ \mathbf{0} & \mathbf{0} & \mathbf{I} & \mathbf{0} \\ \mathbf{0} & \mathbf{0} & -(\mathbf{p}_{II} - \mathbf{x}_3)\times & \mathbf{I} \end{bmatrix} \tag{4}$$

If perturbation is applied to Eq. 3,

$$\cancel{\mathbf{A}_0\vartheta_0} + \mathbf{A}_0\delta\vartheta + \delta\mathbf{A}\vartheta_0 + \cancel{\delta\mathbf{A}\delta\vartheta} = \cancel{\mathbf{F}_0} + \delta\mathbf{F} \tag{5}$$

where terms with 0 subscripts are reference conditions. Eq. 6 is the linearised equilibrium equation around a reference condition after neglecting higher order terms and cancelling the reference condition. The term $\mathbf{A}_0\delta\vartheta$ gives the perturbation of internal loads with an arms matrix at reference configuration whereas $\delta\mathbf{A}\vartheta_0$ term is responsible for the stiffness contribution due to pre-stress of the beam element, which can be omitted if the static loads are not extreme. The final linearised form is then:

$$\mathbf{A}_0\delta\vartheta = \delta\mathbf{F} \tag{6}$$

Now the internal loads should be linked to internal strains. Considering that it is more convenient to provide constitutive law in the material reference frame, internal forces given can be expressed in the beam frame as ;

$$\vartheta = \mathcal{D}\psi = \mathcal{R}\tilde{\mathcal{D}}\mathcal{R}^T\psi \tag{7}$$

where $\mathcal{R}$ and $\tilde{\mathcal{D}}$ are the rotation and constitutive law matrices having the contributions from two evaluation points and similarly ϑ and ψ are the internal load and strain vectors at the evaluation points.

(8a)

$$\mathcal{R} = diag([\mathbf{R}_I \;\; \mathbf{R}_I \;\; \mathbf{R}_{II} \;\; \mathbf{R}_{II}]) \;\; , \;\; \tilde{\mathcal{D}} = diag([\tilde{\mathbf{D}}_I \;\; \tilde{\mathbf{D}}_{II}])$$

$$\vartheta = [\vartheta_I^T \;\; \vartheta_{II}^T]^T \;\; , \;\; \psi = [\psi_I^T \;\; \psi_{II}^T]^T \tag{8b}$$

Using updated Lagrangian, i.e. reference load, approach, the perturbation of internal loads ϑ is;

$$\delta\vartheta = \delta\mathcal{R}\tilde{\mathcal{D}}\mathcal{R}_0^T\psi_0 + \mathcal{R}_0\tilde{\mathcal{D}}\mathcal{R}^T\delta\psi \tag{9}$$

where terms with 0 index represents reference conditions. For a rotation matrix $\mathbf{R}$ and corresponding linearised rotation angle φ, Eq. 9 is rearranged as,

$$\delta\vartheta = \mathcal{R}_0\mathcal{D}\mathcal{R}_0^T\delta\psi \tag{10}$$

where ϑ_0 and $\psi_\mathbf{0}$ are the reference internal forces and strains and $\times$ represents the matrix from of a vector product operation as before. Considering that in rotor blades, the magnitude of centrifugal loads are significantly higher than that of other forms of external loads; only tension forces due to rotation ($\mathbf{t_0}$) at evaluation points are considered as reference internal loads. Finally, $\delta\psi$ can be written using shape functions and linearised strain for the perturbation variables $\mathbf{x}_i$ and φ_i of the i^{th} node

(11)

$$\delta\psi = \begin{bmatrix} \delta\varepsilon_I \\ \delta\kappa_I \\ \delta\varepsilon_{II} \\ \delta\kappa_{II} \end{bmatrix} = \begin{bmatrix} N'_{Ii}\mathbf{I} & \mathbf{p}'_{0I}\times N_{Ii} - N'_{Ii}\mathbf{f}_i\times \\ 0 & N'_{I,i}\mathbf{I} \\ N'_{IIi}\mathbf{I} & \mathbf{p}'_{0I}\times N_{IIi} - N'_{IIi}\mathbf{f}_i \\ 0 & N'_{IIi}\mathbf{I} \end{bmatrix} \begin{bmatrix} \mathbf{x}_i \\ \varphi_i \end{bmatrix} = \mathbf{N}_i \begin{bmatrix} \mathbf{x}_i \\ \varphi_i \end{bmatrix}$$

with $\mathbf{f} = \mathbf{R}\tilde{\mathbf{f}}$, where $\tilde{\mathbf{f}}$ is the offset of the material frame from the blade reference frame and shape functions (N):

(12)

$$N_1(\xi) = \frac{\xi(\xi-1)}{2} \qquad N_2(\xi) = 1-\xi^2 \qquad N_3(\xi) = \frac{\xi(\xi+1)}{2}$$

where $\xi = -1,0,1$ are the points on local coordinate (ξ) corresponding to three nodes.

Finally, the internal loads ϑ are related to strains ψ by a linear elastic constitutive law $\vartheta_k = \mathbf{D}_k\psi_k$ at two evaluation points $\xi_{I,II} = -1/\sqrt{3}, 1/\sqrt{3}$. The model is composite ready and can be fully populated. To illustrate the input here, an isotropic cross section with double symmetry is considered. In this case, the 6×6 material matrix $\mathbf{D}$ about its principal axis has the following form;

$$\mathbf{D} = diag([EA \;\; GA_y \;\; GA_z \;\; GJ \;\; EI_y \;\; EI_z]) \tag{13}$$

where EA is the axial stiffness, GA_y and GA_z are the shear stiffness about principal axes, GJ is the torsional stiffness, EJ_y and EJ_z are the bending stiffnesses about bending principal axes. Then the 18×18 stiffness matrix can be written for the three node beam element as:

$$\mathbf{F} = \mathbf{K}\begin{bmatrix}\mathbf{x}_1 & \varphi_1 & \mathbf{x}_2 & \varphi_2 & \mathbf{x}_3 & \varphi_3\end{bmatrix}^T \tag{14}$$
$$\text{for } \mathbf{K} = \mathbf{A}_0\mathcal{R}_0\mathcal{D}\mathcal{R}_0^T diag([\mathbf{N}_1\mathbf{N}_2\mathbf{N}_3])$$

It should be noted that this is the stiffness matrix of a single beam element. A global matrix should be formed if more than one beam element is needed. For further reading on the model, please refer to Refs. [15,16].

Mass and Inertia

The mass and inertia distribution of the beam and other associated elements such as batteries are realised as concentrated elements. As given in Fig. 2, the lumped mass m having a 3×3 inertia matrix $\mathbf{J_{CM}}$ are assigned to nodes with offsets $\mathbf{f_{CM}}$, which represent the inertial characteristics of the volume in the vicinity of the corresponding node. Writing force and moment equations in perturbation form and collecting in matrix form yields:

$$\begin{bmatrix} \mathbf{F_{in}} \\ \mathbf{M_{in}} \end{bmatrix} = -\begin{bmatrix} m\mathbf{I} & m\mathbf{f_{CM}}\times^T \\ m\mathbf{f_{CM}}\times & \mathbf{J_n} \end{bmatrix} \begin{bmatrix} \ddot{\mathbf{x}} \\ \ddot{\varphi} \end{bmatrix} \tag{15}$$

Wing Unsteady Aerodynamics

The unsteady aerodynamics model is based on the unsteady aerodynamics of the airfoil sections explained in Ref. [17]. Consider the equations of motion of an airfoil:

$$\mathbf{M}\ddot{\mathbf{x}} + \mathbf{C}\dot{\mathbf{x}} + \mathbf{K}\mathbf{x} = \mathbf{f}$$

In the above equation, $\mathbf{x} = [w \;\; \alpha \;\; \xi]^T$ is the state vector for plunging w, pitching α and augmented state ξ. $\mathbf{f}_{nl}$ is the nonlinear forcing due to cubic spring force. and $\mathbf{K}$, $\mathbf{C}$, and $\mathbf{M}$ are linear stiffness, damping, and mass matrices including unsteady aerodynamics matrices ($\mathbf{M}_{aero}, \mathbf{C}_{aero}, \mathbf{K}_{aero}$). The stiffness and mass terms are obtained using the beam model as explained above. Therefore only aerodynamic terms will be retained here, which are given as:

(16)

$$\mathbf{M}_{aero} = \pi\rho b^2 \begin{bmatrix} 1 & -ab & 0 \\ -ab & (\frac{1}{8}+a^2)b^2 & 0 \\ 0 & 0 & 1 \end{bmatrix}$$

$$\mathbf{C}_{aero} = 2\pi\rho b^2 U$$

$$\begin{bmatrix} \frac{c_5}{b} & (1+c_5)\left(\frac{1}{2}-a\right) & \frac{c_6}{b} \\ -(a+\frac{1}{2})c_5 & \left(\frac{1}{2}-a-\frac{c_5}{2}\left(\frac{1}{4}-a^2\right)\right)\frac{b}{2} & -U(a+\frac{1}{2})c_6 \\ \frac{-1}{2\pi\rho b^3 U} & \left(a-\frac{1}{2}\right)\frac{1}{2\pi\rho b^2 U} & (c_2+c_4)\frac{U}{2\pi\rho b^3 U} \end{bmatrix}$$

$$\mathbf{K}_{aero} = 2\pi\rho b U^2$$

$$\begin{bmatrix} 0 & c_5 & U c_2 c_4 (c_1+c_3) \\ 0 & -(\frac{1}{2}+a)c_5 b & -(a+\frac{1}{2})c_2 c_4 (c_1+c_3) \\ 0 & -\frac{U}{2\pi\rho b^2 U^2} & c_2 c_4 \frac{U^2}{2\pi\rho U^2 b^2} \end{bmatrix}$$

where the constants are: $c_0 = 1.0$, $c_1 = 0.165$, $c_2 = 0.0455$, $c_3 = 0.335$, $c_4 = 0.3$, and the dependent variables $c_5 = c_0 - c_1 - c_3$, $c_6 = c_1 c_2 + c_3 c_4$.

The above system is formulated for airfoil sections. The pitch and plunge degrees of freedom can be directly inserted into the equations of motion of the system. The augmented state (ξ) is added based on Wagner's function for arbitrary (i.e. not only valid for simple harmonic motion) airfoil motion. For each wing section, an augmented state was added into the equations of motion. These extra states will lead to zero valued eigenvalues, which should be ignored in the final results. On a final note about using the Wagner's function for arbitrary airfoil motion is that it allows to identify damping at any flight speed.

Propeller

The propeller model is based on Reed's classical whirl flutter model for an arbitrary number of propellers. Therefore it is worth revisiting the original model. The 2-DOF Reed's whirl flutter model [6], as visualised in Fig. 3, is a well-known aeromechanical model in the literature. The dynamical system consists of the rotor (propeller), forming the gyroscopic and aerodynamic forces, supported horizontally by a pylon that is pivoted at some wing attachment point. The spin axis of the propeller is oriented more or less into the direction of the freestream flight velocity V with angular perturbations from this vector in pitch θ and yaw ψ. If we denote the angular moment of inertia of the pylon (including the diametral moment of inertia of the rotor and nacelle inertia) about the pivot point as I_n and the polar moment of inertia of the rotor as I_x. Then, the following equations of motion can be written:

$$\begin{bmatrix} I_n & 0 \\ 0 & I_n \end{bmatrix} \begin{Bmatrix} \ddot{\theta} \\ \ddot{\psi} \end{Bmatrix} + \begin{bmatrix} C_\theta & -I_x\Omega \\ I_x\Omega & C_\psi \end{bmatrix} \begin{Bmatrix} \dot{\theta} \\ \dot{\psi} \end{Bmatrix} + \begin{bmatrix} K_\theta & 0 \\ 0 & K_\psi \end{bmatrix} \begin{Bmatrix} \theta \\ \psi \end{Bmatrix} = \begin{Bmatrix} M_\theta \\ M_\psi \end{Bmatrix} \quad (17)$$

where M_θ and M_ψ are the applied moments in pitch and yaw, taken about the pivot point, arising from the aerodynamic loads. These terms can be formulated in the form of perturbational aerodynamic loads using the Strip Theory, which are expressed as follows:

$$M_\theta = \frac{N_b}{2} K_a R \left[-(A_3 + a^2 A_1)\frac{\dot{\theta}}{\Omega} - A_2'\psi + aA_1'\theta \right], \quad (18)$$

$$M_\psi = \frac{N_b}{2} K_a R \left[-(A_3 + a^2 A_1)\frac{\dot{\psi}}{\Omega} + A_2'\theta + aA_1'\psi \right] \quad (19)$$

where the constants are as a function of the Advance Ratio (μ):

$$A_1 = \frac{c}{R}\int_0^1 \frac{\mu^2}{\sqrt{\mu^2+\eta^2}} d\eta, \quad A_1' = \mu A_1, \quad (20)$$
$$A_2' = \frac{c}{R}\int_0^1 \frac{\mu^2\eta^2}{\sqrt{\mu^2+\eta^2}} d\eta, \quad , A_3 = \frac{c}{R}\int_0^1 \frac{\eta^4}{\sqrt{\mu^2+\eta^2}} d\eta$$

which can be numerically integrated to obtain the aerodynamic damping (C_{areo}) and stiffness (K_{areo}) matrices. These degrees of freedom are added to the already existing wing degrees of freedom.

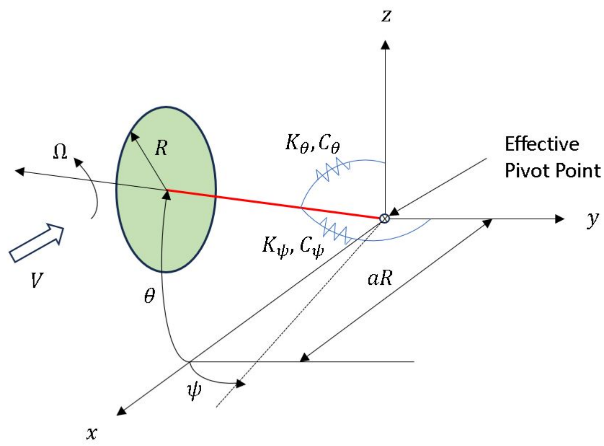

Figure 3: Reed's 2-dof flutter model [6].

The propellers can be attached with an offset to the elastic axis of the wing, which causes dynamical coupling with the wing dynamics. This was directly adopted from Ref. [2], and stated follows:

$$\begin{bmatrix} M_P & S_{\alpha,P} & S_{\theta,P} & 0 \\ S_{\alpha,P} & I_{\alpha,P} & I_{\theta,P} & 0 \\ S_{\theta,P} & I_{\theta\alpha,P} & 0 & 0 \\ 0 & 0 & 0 & 0 \end{bmatrix} \begin{bmatrix} \ddot{w} \\ \ddot{\theta}_x \\ \ddot{\theta} \\ \ddot{\psi} \end{bmatrix} + \begin{bmatrix} 0 & 0 & 0 & 0 \\ 0 & 0 & 0 & I_x\Omega \\ 0 & 0 & 0 & 0 \\ 0 & -I_x\Omega & 0 & 0 \end{bmatrix} \begin{bmatrix} \dot{w} \\ \dot{\theta}_x \\ \dot{\theta} \\ \dot{\psi} \end{bmatrix} = \begin{bmatrix} F_z \\ M_x \\ M_\theta \\ M_\psi \end{bmatrix} \quad (21)$$

where definitions of these terms can be found in Ref. [2] and the matrices already provided in Eq. 17 are not included in Eq. 21.

Results and Discussion

This section verifies the suggested method and provides parametric analysis to demonstrate its benefit in aeroelastic analysis of distributed propulsion aircraft.

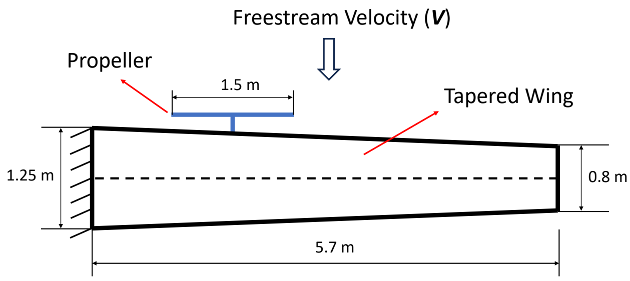

Figure 4: General properties of the tapered wing-propeller model.

Analysis Model

The analysis model is based on the twin-engine Tecnam P2006T aircraft based on the date reported in Ref. [2]. This model mainly consists of a tapered wing and a propeller as shown in Fig. 4. The propeller is attached to the leading-edge side of the wing. As an overview, the wing has a 5.7 meter half-span and the propeller has a 1.524 meter rotor diameter. Root and tip chords are also 1.25 meter and 0.8 meter, respectively. The whole wing data is provided in Table1, and the propeller data is given in Table 2.

The wing structural model was created with five beam elements using the finite volume method. For creating the wing aerodynamic model, unsteady aerodynamics theory based on Wagner's function was used as explained in the method section. An extended version of Reed's model for an arbitrary number of propellers was also employed for the aeroelastic modelling of propeller. The whole wing and propeller data were used to model a single engine wing in order to verify the proposed method by the authors. The model was then modified to demonstrate its use in distributed propulsion aircraft analysis.

Parameter	Value
Wing Span	11.4 m
Root chord	1.25 m
Tip chord	0.8 m
Thickness to chord	15%
Radius of Gyration	25% chord
Elastic Axis from LE	50% chord
CG from LE	50% chord
Aerodynamic Centre from LE	25% chord
Bending Rigidity	7×10^5 N m^2
Torsional Rigidity	2×10^5 N m^2
Lift curve slope	2π
Cruise Speed	120 knots
Altitude	2440 m

Table 1: Baseline Wing Data [2].

Parameter	Value
Number of blades	3
Rotor diameter	1.524 m
Blade chord	0.0924 m
Cruise RPM	2250
Rotor mass	8 kg
Motor-nacelle mass	35 kg
Position of rotor CG	1.16 m
Position of motor CG	0.86 m
Pitch non-rotating Frequency	7 Hz
Yaw non-rotating Frequency	7 Hz
Pitch damping ratio	0.005
Yaw damping ratio	0.005
Engine Position	31%

Table 2: Baseline Propeller Data [2].

Wing Model Convergence

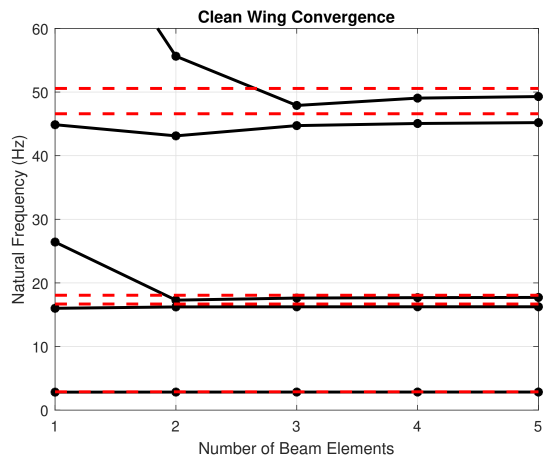

Figure 5: Convergence of the clean wing natural frequencies.

A convergence study on the clean wing has been conducted in terms of natural frequency. As shown in Fig. 5, natural frequencies of the clean wing model start to converge around three beam elements without the necessity of the higher number of elements. This is one of the important advantages of using a 3-node finite volume beam compared to the other numerical methods.

It is found that higher modes converge slowly because of the higher number of element requirements for them, which is also similar to the beam element convergence study in the finite element method. It is worth stating that the lower modes which dominate the wing flutter have a higher potential to be coupled with the propeller. This coupled aeroelastic behaviour of the tapered wing - propeller model can be captured with even two beam elements. However, five beam elements have been used to analyse the position of the propeller and the number of propellers in the rest of this study.

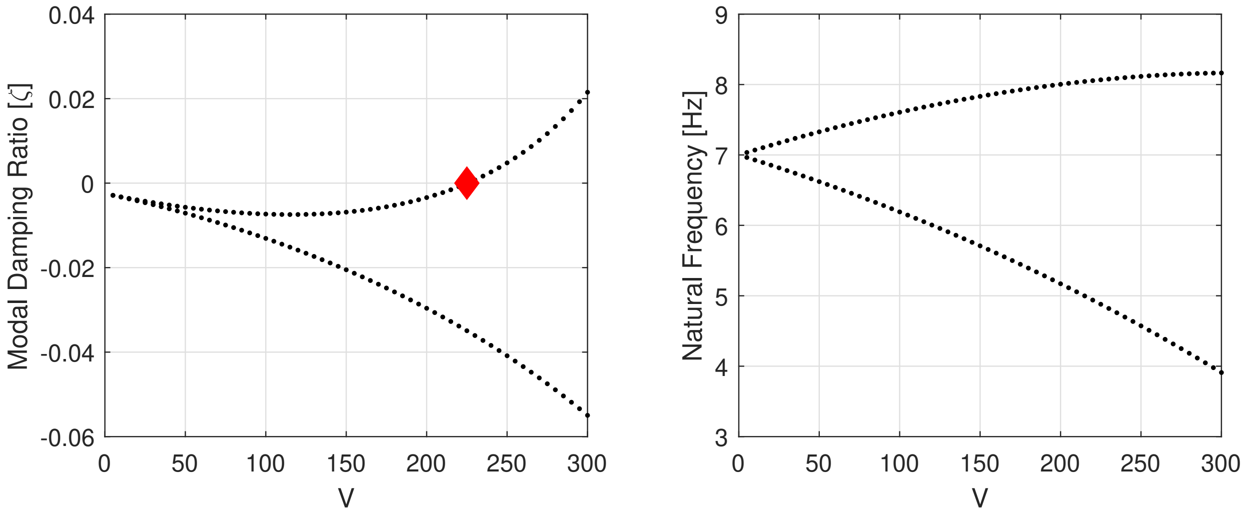

a) Only propeller including propeller aerodynamics

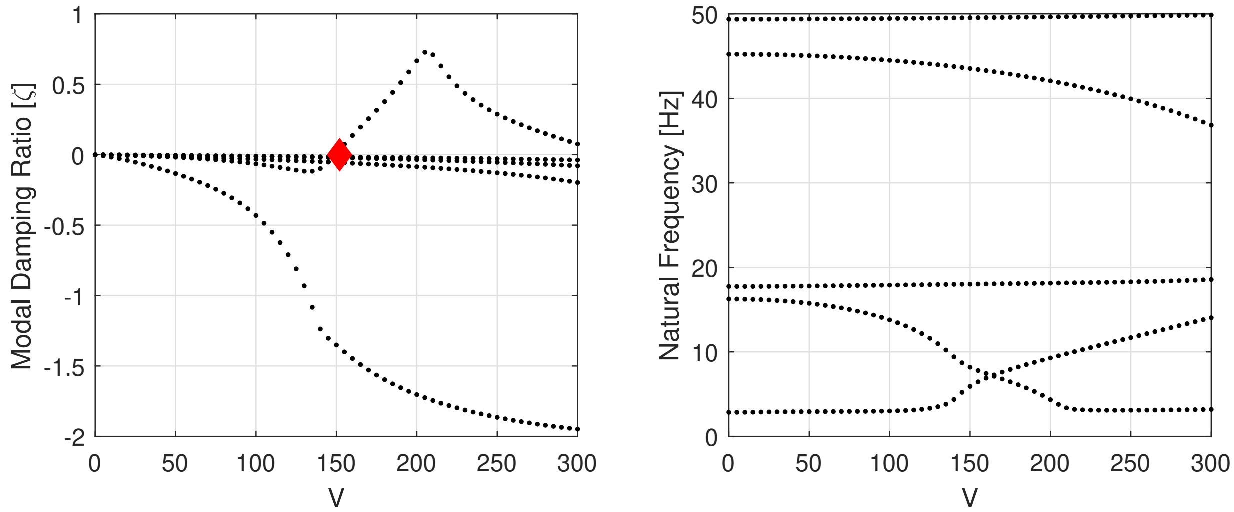

b) Only wing including wing aerodynamics

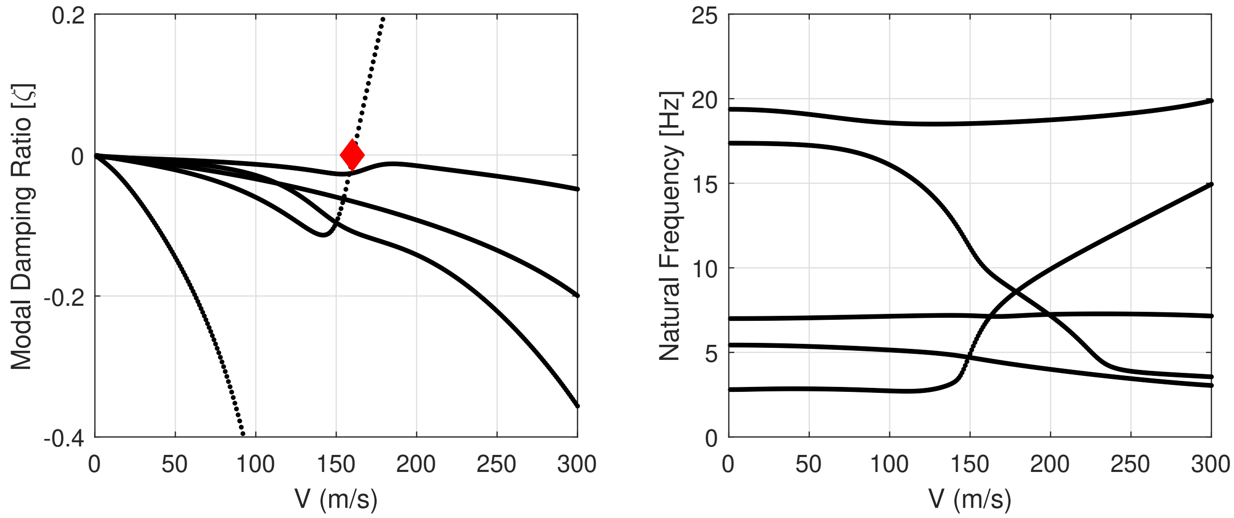

c) Wing and propeller including wing and propeller aerodynamics

Figure 6: $V-g$ and $V-\omega$ plots for the verification of the results with results summarised in Table 3.

Flutter Verification

The model developed using the method was successfully verified against the results in Ref. [2] for the three cases which are clean wing, only propeller and propeller and wing. The windmilling condition was applied assuming a constant propeller advance ratio of $J = 1.96$ It should be noted that this advance ratio is different that μ used in Reed's model.

Natural frequency ($V - \omega$) and modal damping (V-g) data with respect to the airspeed are given in Fig. 6 for the three cases, which are (i) only propeller, (ii) only wing and (iii) coupled wing and propeller. When analysing the propeller (i) and wing (ii) dynamics separately, it is found that the critical speed of the whirl flutter (225 m/sec) is significantly higher than the wing flutter (149 m/sec). On the other hand, the critical speed in the coupled wing-propeller aeroelastic model becomes 160 m/sec, which is close to the only wing model. These results clearly show that the critical speed due to the flutter instability is mainly dominated by wing dynamics. Table 3 compares the results with those reported in Ref. [2]. Overall, there is a good correlation between the results of the reference study and the current study in terms of critical speed. The difference between them is found to be at an acceptable level.

Case	Critical Speed	Reference[1]
Clean Wing	149 m/s	152 m/s
Only Propeller	225 m/s	221 m/s
Propeller and Wing	160 m/s	152 m/s

[1]Obtained from Ref. [2]

Table 3: Comparison of critical speeds for three cases.

Effect of Engine Spanwise Location

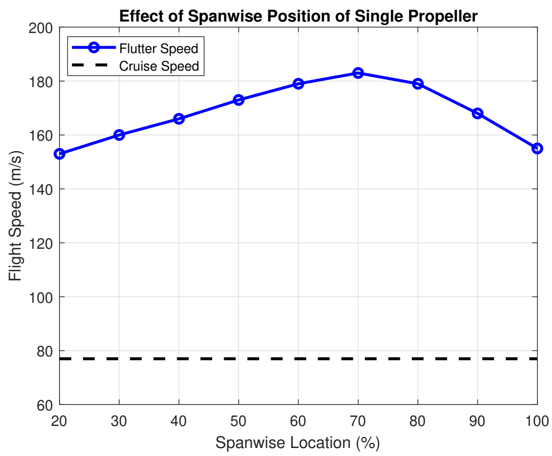

Figure 7: Effect of spanwise location of the propeller on flutter speed.

In order to investigate the flutter speed sensitivity to engine spanwise location, the position of the propeller was shifted from the wing root to the wing tip. As seen in Fig. 7, flutter speed is lower at the wing root and wing tip, whereas it reaches the maximum level at the 70 percent spanwise location. This analysis mainly demonstrates how quickly the model can be updated and the parametric studies can be done in the early design stages of wing-propeller models.

Multi-Engine Layouts

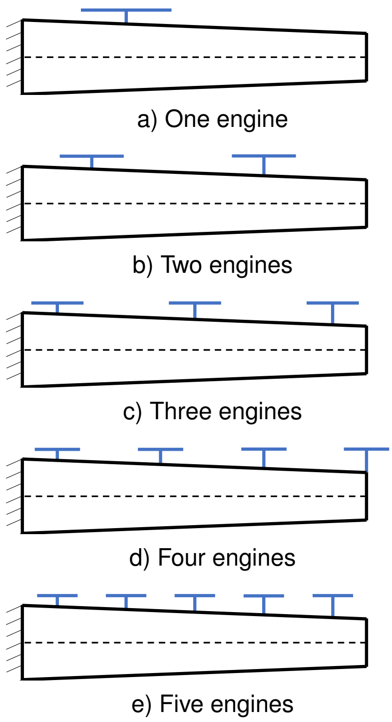

Figure 8: Distributed propulsion configurations.

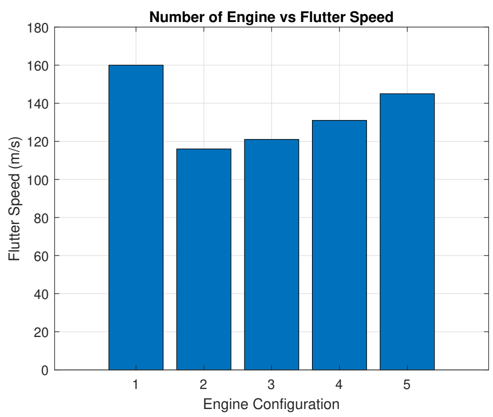

Figure 9: Effect of number of engine on flutter speed.

The method is now applied to different number of engines to analyse the flutter speeds of distributed propulsion aircraft. To do this analysis, the thrust is kept the same by assuming the same total area of the propeller. Therefore the area of the single engine is divided by the number of propellers. This requires that the radius is scaled by the number of engines $\sqrt{N_p}$. It is assumed that the other parameters such as mass and length reported in Table 2 are also proportional to the radius of the propeller. Therefore, they are scaled down accordingly as seen in Fig. 8. The rotational speed of propellers for each configuration were adjusted for 0.7 blade tip mach number. The critical speeds for the five cases are reported in Fig. 9. Number of engines varies from one to five in the five cases. Interestingly, only one engine provides the highest flutter speed, while two engines lead to the lowest flutter speed.

Conclusions

An aeroelastic model of distributed propulsion aircraft at a minimum required complexity level was developed and presented by combining the dynamics of wing and propellers. Finite volume method-based beam formulation and unsteady aerodynamics theory based on Wagner's function have been used to create the structural and aerodynamic model of the wing, respectively. An extended version of classical Reed's model is also used for the aeroelastic modelling of the multi-propeller.

It was shown that the model can predict the coupled aeroelastic behaviour of distributed propulsion aircraft due to the whirl flutter and wing flutter instabilities. The numerical model validation was also successfully conducted by comparing critical speeds with the reference studies in the literature. It is important to point out that this model can be helpful for aeroelastic analysis and optimisation in the early design stages because of not need sophisticated and expensive commercial software. The presented study highlights the importance of coupled aeroelastic analysis of the distributed propulsion aircraft so as to capture the dynamic response accurately. Authors plan to merge the developed tool with urban air mobility sizing tools. This will help to include flutter and whirl flutter in early design process together with other design requirements and constraints.

Acknowledgement

Authors greatly acknowledge the travel support provided by Leonardo Helicopters to present this work.

Copyright Statement

References

[1] W. Johnson and C. Silva. Nasa concept vehicles and the engineering of advanced air mobility aircraft. *The Aeronautical Journal*, 126(1295):59–91, 2022.

[2] V. Q. Liu Xu. Propeller-wing whirl flutter. Master's thesis, TU Delft, 2020.

[3] Christian B. Hoover, Jinwei Shen, Andrew R. Kreshock, Bret Stanford, David J. Piatak, and Jennifer Heeg. *Whirl Flutter Stability and Its Influence on the Design of the Distributed Electric Propeller Aircraft X-57*.

[4] Guru P. Guruswamy. Dynamic aeroelasticity of wings with tip propeller by using navier–stokes equations. *AIAA Journal*, 57(8):3200–3205, 2019.

[5] Nils Böhnisch, Carsten Braun, Stephan Koschel, and Pier Marzocca. *Whirl Flutter for Distributed Propulsion Systems on a Flexible Wing*.

[6] Richard L. Bielawa. *Rotary Wing Structural Dynamics and Aeroelasticity*. AIAA, Washington, DC, 2nd edition, 2005.

[7] Christopher Mair, Djamel Rezgui, and Branislav Titurus. Nonlinear stability analysis of whirl flutter in a rotor-nacelle system. *Nonlinear Dynamics*, 94:2013–2032, 2018. doi:10.1007/s11071-018-4472-y.

[8] Eric Hathaway and Farhan Gandhi. Design optimization for improved tiltrotor whirl flutter stability. *Journal of the American Helicopter Society*, 52(2):79–89, April 2007. https://doi.org/10.4050/JAHS.52.79.

[9] Jiří Čečrdle. 1 - introduction to aircraft aeroelasticity and whirl flutter. In Jiří Čečrdle, editor, *Whirl Flutter of Turboprop Aircraft Structures*, pages 1–12. Woodhead Publishing, Oxford, 2015.

[10] Wilmer H. Reed. Propeller-rotor whirl flutter: A state-of-the-art review. *Journal of Sound and Vibration*, 4(3):526–544, 1966.

[11] Wayne Johnson. Dynamics of tilting proprotor aircraft in cruise flight. 1974.

[12] Alessandro Cocco, Stefano Mazzetti, Pierangelo Masarati, Stefan van't Hoff, and Bart Timmerman. Numerical whirl–flutter analysis of a tiltrotor semi-span wind tunnel model. *CEAS Aeronautical Journal*, 1:923–938, 2022. doi:10.1007/s13272-022-00605-2.

[13] Gianni Cassoni, Aleassandro Cocco, Aykut Tamer, Andrea Zanoni, and Pierangelo Masarati. Tiltrotor whirl-flutter stability investigation using lyapunov characteristic exponents and multibody dynamics. In *European Rotorcraft Forum*, Winterthur, CH, 2022.

[14] Leonardo helicopters (last accessed aug 2023). https://www.leonardo.com/en/news-and-stories-detail/-/detail/leonard-clea-aviation-programme.

[15] Gian Luca Ghiringhelli, Pierangelo Masarati, and Paolo Mantegazza. A multi-body implementation of finite volume beams. *AIAA Journal*, 38(1):131–138, January 2000. doi:10.2514/2.933.

[16] Aykut Tamer and Pierangelo Masarati. Linearized structural dynamics model for the sensitivity analysis of helicopter rotor blades. In *Ankara International Aerospace Conference*, Ankara, TR, September 11–13 2013.

[17] John W. Edwards, Holt Ashley, and John V. Breakwell. Unsteady aerodynamic modeling for arbitrary motions. *AIAA Journal*, 17(4):365–374, April 1979. doi:10.2514/3.7348.